Supplementary Information

Aerosol synthesis of thermally stable porous noble metals and alloys by using bi-functional templates

Mateusz Odziomek,[1] Mounib Bahri,[2] Cedric Boissiere,[1] Clement Sanchez,[1] Benedikt Lassalle-Kaiser,[3] Andrea Zitolo,[3] Ovidiu Ersen,[2] Sophie Nowak,[4] Cedric Tard,[5] Marion Giraud,[4]* Marco Faustini,[1]* Jennifer Peron[4]*

1. Sorbonne Université, CNRS, Collège de France, PSL Research University, Laboratoire Chimie de la Matière Condensée de Paris, LCMCP, 4 Place Jussieu, F-75005, Paris, France

2. IPCMS-UMR 7504 CNRS, Université de Strasbourg, 23 Rue du Loess, BP 43-67034, Strasbourg Cedex 2, France

3. Synchrotron SOLEIL, L'Orme des Merisiers, Saint-Aubin, 91192 Gif-sur-Yvette, France

4. Université de Paris, ITODYS, CNRS, UMR 7086, 15 rue J-A de Baïf, F-75013 Paris, France

5. LCM, CNRS, Ecole polytechnique, Institut Polytechnique de Paris, France

Experimental Section

Chemicals

$IrCl_3*xH_2O$ (98%) was purchased from Alfa Aesar, $RhCl_3*xH_2O$ (98%), $RuCl_3*xH_2O$ (98%) $H_2PtCl_6*H_2O$ and $PdCl_2$ from Sigma Aldrich. PMMA latex beads were synthesized by radical polymerization from methyl methacrylate following the protocol described in ref. 1. 11 wt% dispersion of 300 nm (size measured by DLS) PMMA beads in water was used for the hybrid materials preparation. PS latex beads were synthesized by radical polymerization method from styrene following the protocol described in ref. 2.

Metals preparation

In a typical synthesis: $IrCl_3*xH_2O$, $RhCl_3*xH_2O$ $RuCl_3*xH_2O$ or $PtCl_4$ (1 g) was dissolved in water (27 mL) under stirring. In the case of $PdCl_2$ it was dissolved in HCl solution of pH=2. The 11 wt% PMMA dispersion was then added to the metal containing solution to obtain a final polymer/metal precursor ratio of 33 wt%. After 10 min stirring, the solution was spray-dried with a B-290 atomizer from Büchi. The spray-dryer parameters were set as follows: input temperature: 220 °C, pump flow: 5 mL min^{-1}. The recovered powder was then calcined at a 450 °C for 15 min under flow of nitrogen or air. The temperature ramp from ambient to the desired temperature was of 20 °C min^{-1} (unless stated otherwise in the text).

Characterization

SEM–FEG images were obtained using a Zeiss SUPRA 40 FESEM, operating at 3 kV.

STEM-HAADF, energy dispersive x-ray spectroscopy (STEM-EDS) and in-situ observations were performed using a JEOL 2100 F equipped with a spherical aberration probe corrector and operating at 200 kV. EDS mapping was performed using JEOL Silicon Drift Detector (DrySD60GV: sensor size 60 mm^2) with a solid angle of approximately 0.5 srad. In situ STEM calcination was carried out using a

Protochips Atmosphere device. The sample was placed between two micro-electrical-mechanical systems (MEMS)-based closed cell (SiN windows). The temperature and the gas flow in the cell are controlled by the heating holder and a gas delivery manifold respectively. All the indicated temperatures are based on the company provided calibration. The sample was dispersed in ethanol and drop-casted on the SiN membrane acting as heater element. The *in situ* experiment was done at atmospheric pressure under N_2 at 450 °C with a change rate of 10 °C/min.

The *ex situ* and *in situ* XRD measurements at different temperatures were carried out using a Panalytical X'pert pro diffractometer equipped with a Co anode (λKα = 1.79031 Å) and a multichannel X'celerator detector. Each pattern was recorded in the θ–θ Bragg–Brentano geometry in the 15°–120° 2θ range (during 40 s each 0.0334°). The high temperature oven chamber was an Anton Paar HTK 1200N and the crucible was made of alumina. The rise in temperature was between 25 and 800 °C, with a measurement every 50 °C.

Physisorption studies were performed with N_2 at 77 K using a Belsorp-max apparatus from MicrotracBEL. Before analysis, the samples were outgassed at 423 K for 12 h under 0.1 Pa. The BET analysis was carried out in the relative pressure range 0.05–0.35. The pore size distribution was calculated by NLDFT method using the Belsorp software.

Thermogravimetric analyses were performed using a Setaram TGA92 under helium from room temperature to 750 ^{o}C with a temperature ramp of 5 K min^{-1} (unless stated otherwise in the text). The FTIR spectra of evolved gaseous products during TG analysis was recorded by Thermoscientific Infra-Red Spectrometer Model IS 10. GC-MS analysis of gaseous products produced during TG analysis was performed by the 403 Aeolos Quadro quadrupole mass spectrometer produced by Netzsch.

Ir L_{III}-edge X-ray absorption spectra were collected in transmission mode at the SAMBA beamline (Synchrotron SOLEIL) at a ring energy of 2.75 GeV and a nominal current of 500 mA. The energy was monochromatized using a sagittally focusing Si 220 monochromator and two Pd-coated mirrors that were used to remove X-rays harmonics. The incoming and transmitted beam intensity was monitored using Ar-filled ionization chambers. *In situ* XAS measurements were performed in a quartz capillary heated by a gas stream blower from room temperature up to 600 °C at the rate of 5 °C/min, and in nitrogen flowing. Data reduction and analysis was performed using the Athena software.

XPS spectra were recorded using a K-Alpha+ spectrometer from Thermofisher Scientific, fitted with a microfocused, monochromatic Al Kα X-ray source (hν = 1486.6 eV; spot size = 400 μm). The pass energy was set at 150 and 40 eV for the survey and the narrow regions, respectively. Spectral calibration was determined by setting the main C 1s (C-C, C-H) component at 284.8 eV.

XANES fitting using LCF program in the Athena program

Since the transformation between the precursor and the metal seems to be a real interconversion between the 2 species, the fit was done according to the following procedure:

1) The room temperature spectrum (before calcination starts) was assigned to spectrum A and the final spectrum (a merged spectrum for all the spectra recorded at temperatures above 700°C when the evolution is no more visible) was assigned to spectrum B.
2) Using the LCF function of Athena, we could perform a linear combination fit with two components (A and B) of the XANES part of each spectrum S recorded at a given temperature. The weight was chosen to be constrained to be between 0 and 1.

$$S = x*A + (1-x)* B$$

3) The values found were gathered in a table and plotted as a function of the calcination temperature.

Supplementary Figures

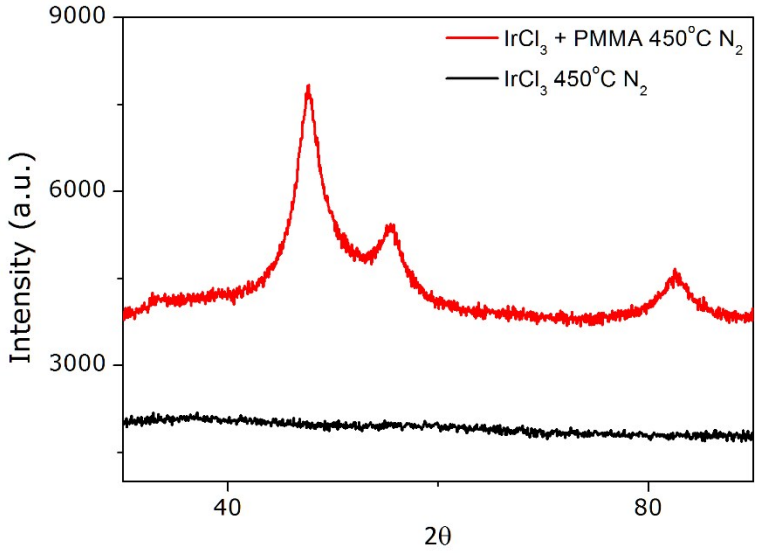

Figure S1 XRD patterns of conventionally dried and calcined at 450 °C in nitrogen: iridium chloride hydrate (black) and iridium chloride mixed with PMMA (red)

In both cases $IrCl_3*xH_2O$ and $IrCl_3*xH_2O$ / PMMA (1:0,33 w/w) were dissolved in water, dried at 130 °C and calcined at the same conditions as spray-dried product. Clearly, the presence of PMMA induces crystallization of metallic Ir.

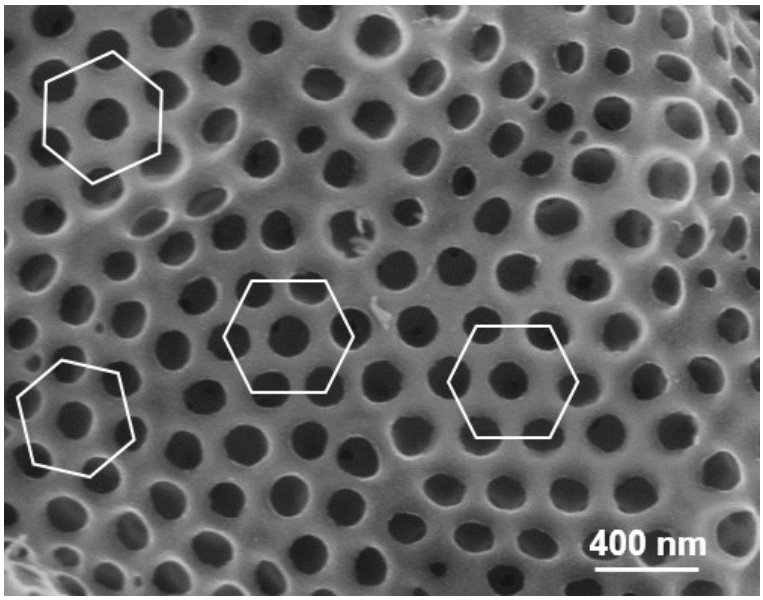

Figure S2 SEM picture of quasi hexagonal arragement of pores formed by latex particles

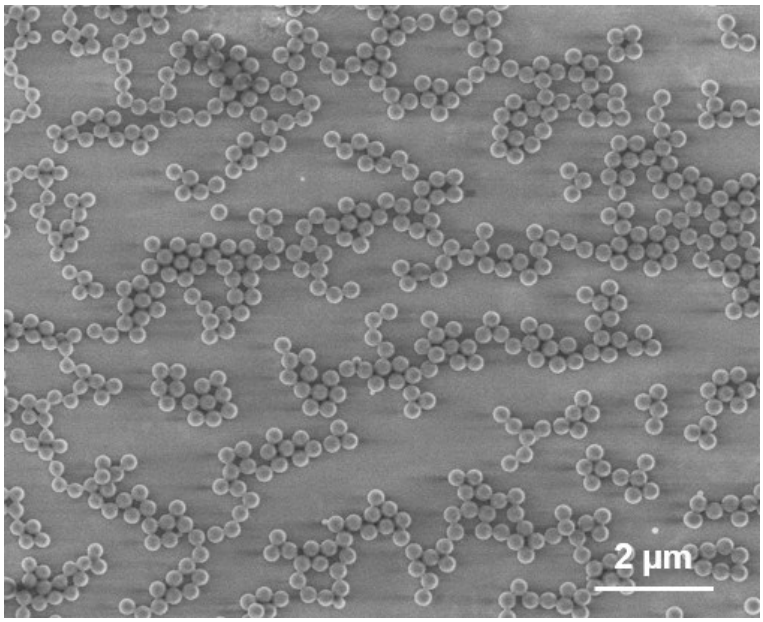

Figure S3 SEM picture of PMMA latex beads utilized in the synthesis

The average particles size measured from SEM pictures was 268,6 ± 5,6 nm. However, it has to be pointed out that the electron beam caused gradual degradation of the beads and their shrinkage. It means that their size in solution could be slightly larger, especially taking into account their possibility of their swelling in the solvent. This can explain the slight difference with the size measured by DLS (300 nm).

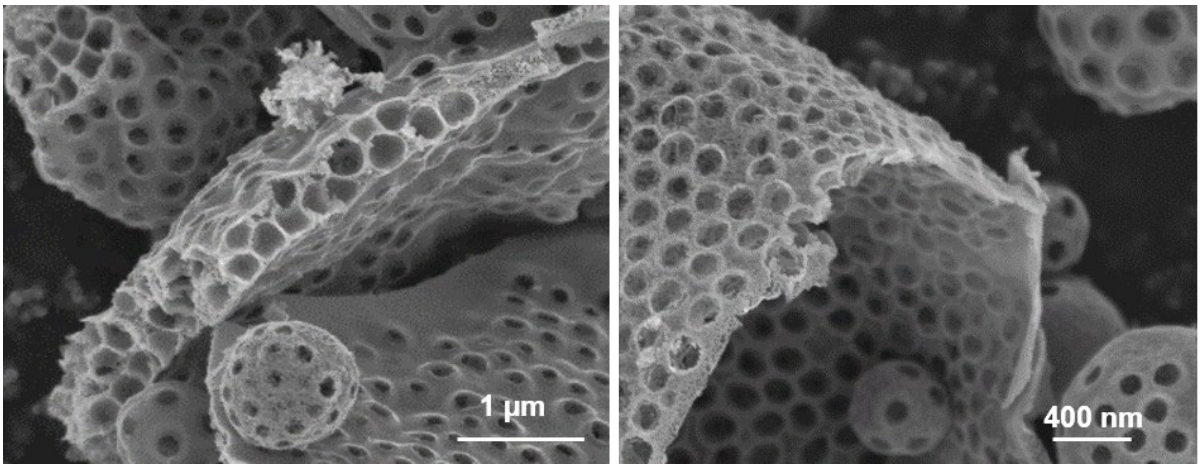

Figure S4 SEM pictures of broken hollow spheres, well exposing the thicknes of the spheres

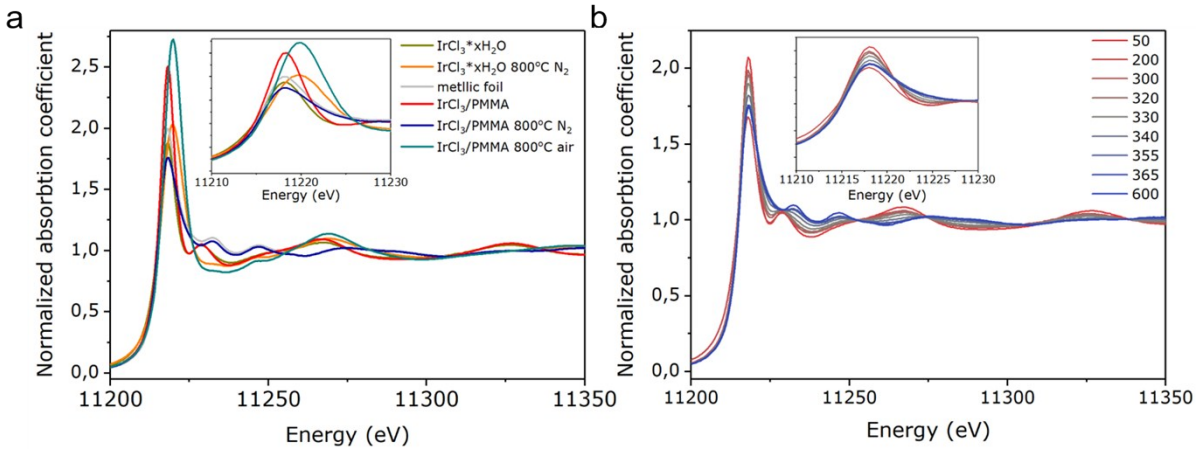

Figure S5 *Ex situ* and *in situ* XANES. a) *ex situ* XANES of spray-dried product and $IrCl_3$ precursor thermally treated at different conditions and compared to metallic iridium foil; b) *in situ* XANES of spray dried product during thermal treatment in nitrogen atmosphere

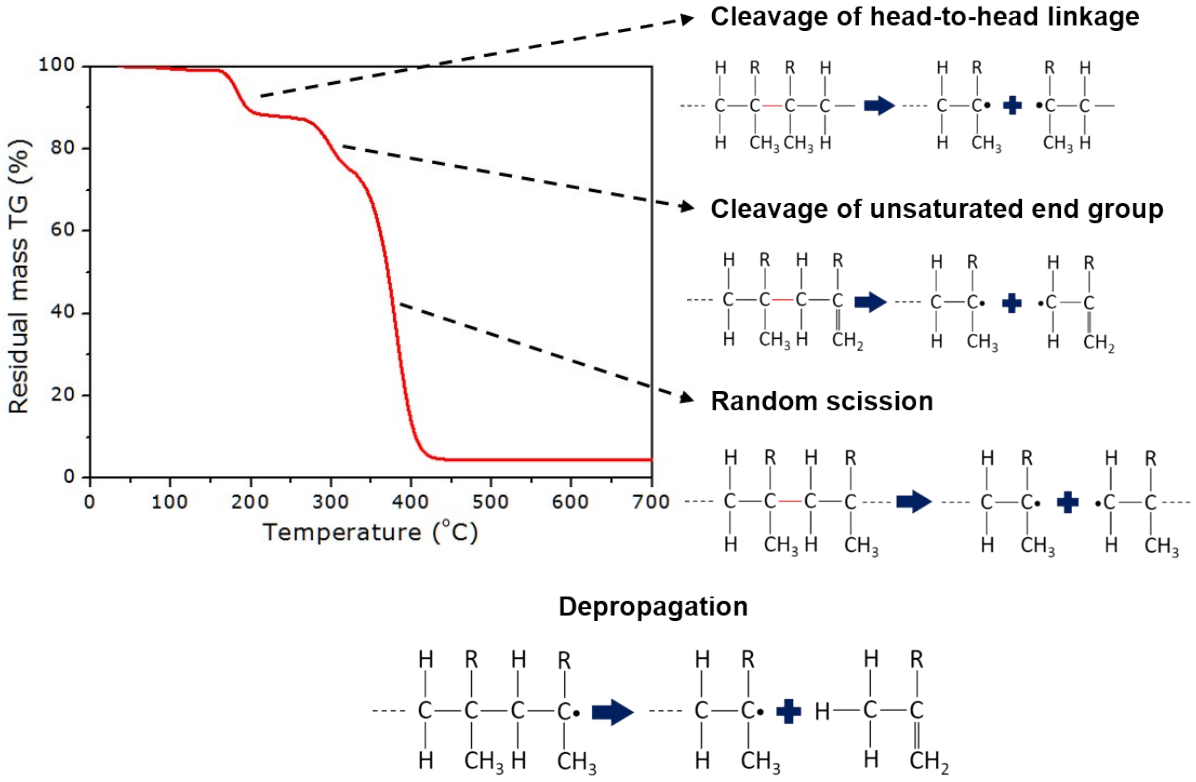

***Figure S6* The mechanism of PMMA depolymerization**. The graph presents TGA of PMMA latex with corresponding decomposition pathways

According to the literature, decomposition of radically polymerized PMMA occurs in 3 stages.[3–5] This is in a good agreement with the TGA of PMMA latex used in this work. Three mass losses are observed and they start at 160 °C, 270 °C and 320 °C (heating rate: 5 °C/min). In each stage the homolytic cleavage of C-C bonds occurs generating radicals. The decomposition at lowest temperature is characteristic to head-to-head bonds in which two alpha carbons are connected together. The following bonds to break at higher temperatures are the unsaturated double bonds at chains ends. Finally, the last ones to break are “normal” bonds within the chain. Each of these cleavages form radicals which undergo one of the following reaction: (i) depropagation producing

volatile MMA monomers; (ii) disproportionation (exchange of hydrogen radical between two initial radicals, and creation of alkane and alkene bonds); iii) radicals recombination.

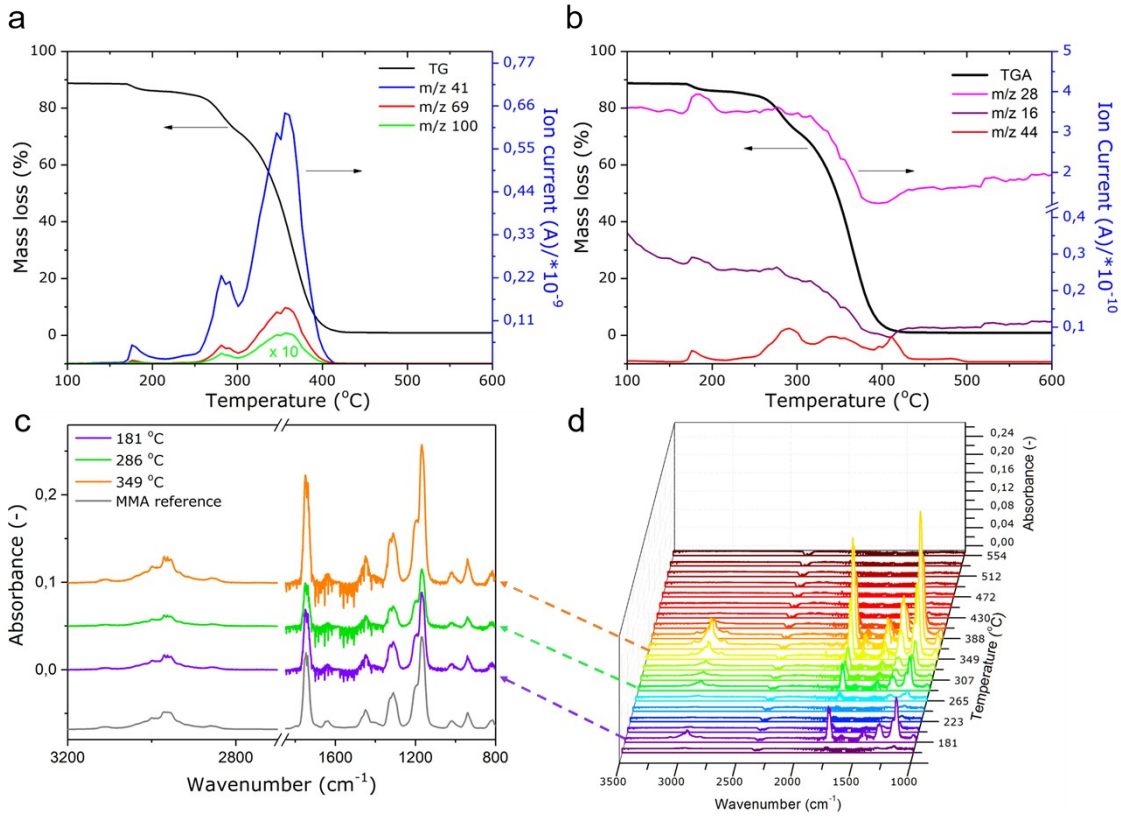

***Figure S7* Analysis of gaseous products generated during TGA of PMMA.** a-b) TGA combined with MS ion currents for pre-selected m/z values; c-d) FTIR spectra of gaseous products evolving with increasing temperatures; the spectra are compared to the reference MMA spectrum (grey)

The TGA shows that decomposition of PMMA latex occurs in 3 consecutive steps (as it is discussed above and in the main text) emphasized by 3 step mass loss in TG curve. Therefore, the FTIR and MS analyses of evolving gases also show three maxima corresponding to 3 stages of mass loss.

MS confirmed evolution of MMA monomers by the detection of species having mass-to-charge ratio of 41, 69 and 100. The last one corresponds to MMA molecule, while the other two are very typical for its fragmentation under ionization.[6,7] We also followed the evolution of peaks corresponding to CO (m/z 28), CH_4 (m/z 16) and CO_2 (m/z 44). Unfortunately, from the beginning of the measurement we observed elevated signals from m/z 16, m/z 32 and m/z 28 which indicate that some amount of O_2 and N_2 was present in the system making the analysis of CO, CO_2 and CH_4 troublesome. Nevertheless, the evolution of CO_2 was observed, at the same temperatures as MMA, together with small but clear peak from CO below 200°C. Both probably partially comes from fragmentation of MMA and partially from alternative decomposition pathways responsible for 6 wt% residue and from oxidation of carbon species.

FTIR analysis further confirmed the detection of almost exclusively MMA monomer in the whole temperature range studied as the spectra agree very well to that of the MMA reference.

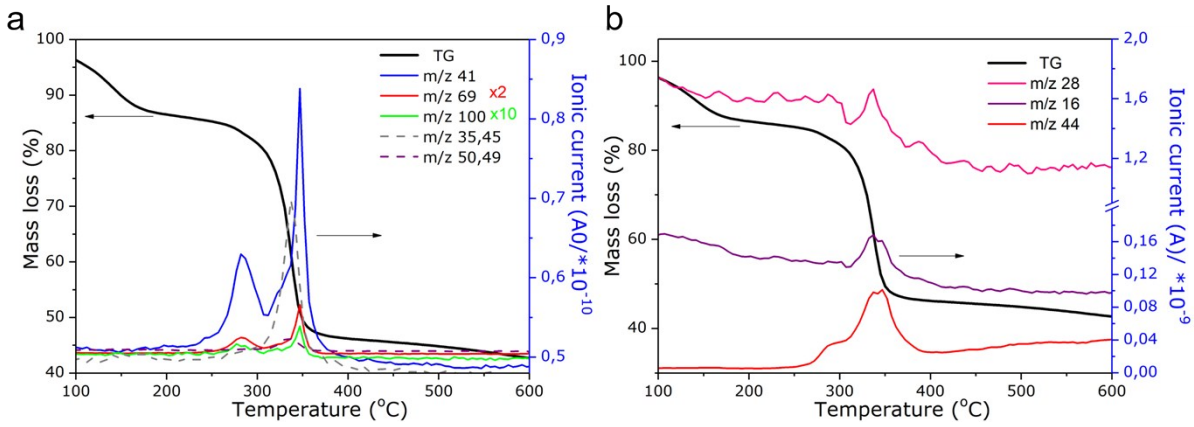

Figure S8 MS of gaseous products evolved during TGA of $IrCl_3$/PMMA hybrid particles

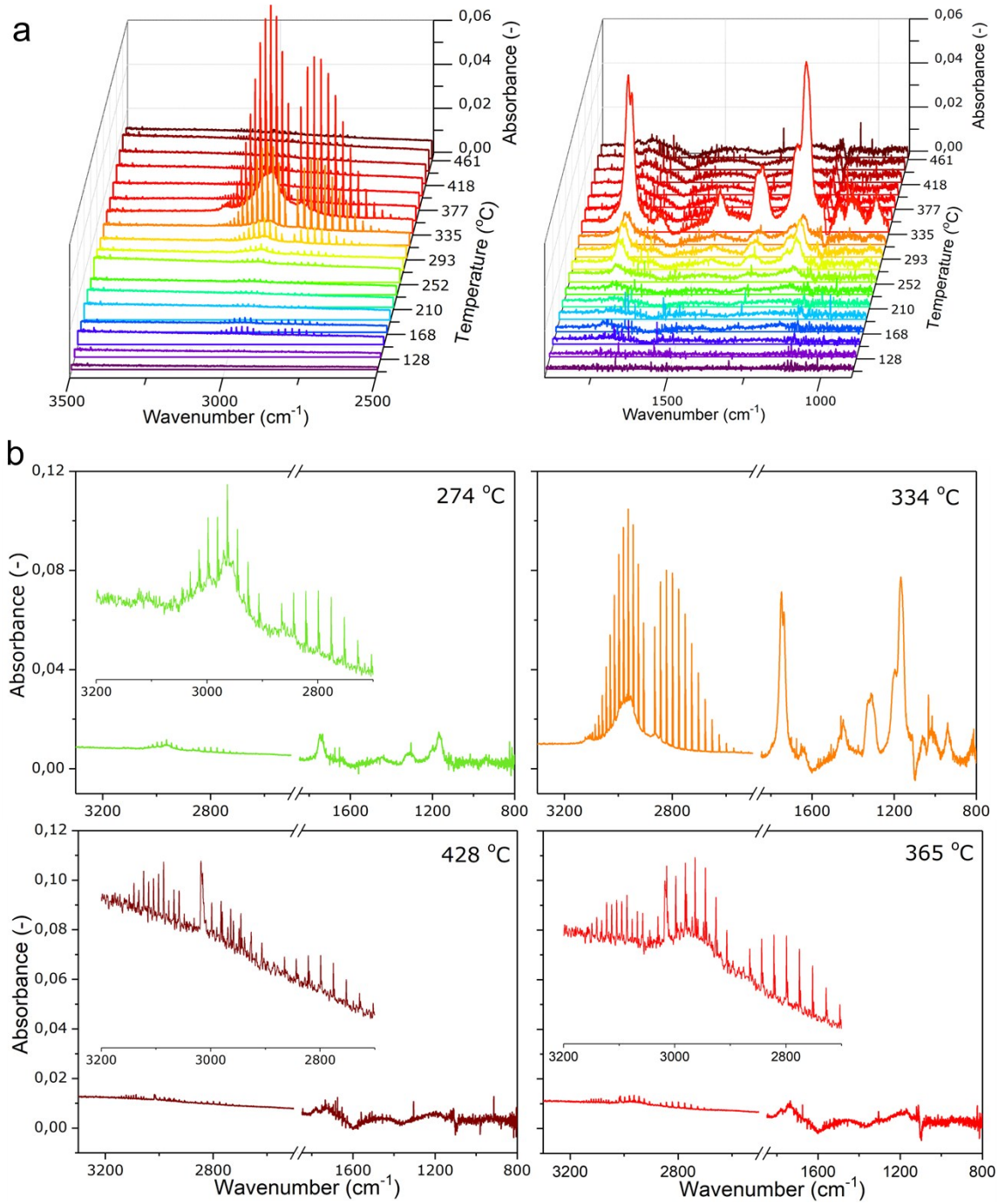

Figure S9 FTIR of gaseous products evolved during TGA of $IrCl_3$/PMMA hybrid particles. (a) Progression of FTIR spectra along with temperature; (b) FTIR spectra corresponding to different temperatures shown separately for clarity; their intensities are not normalized

The TGA of spray-dried hybrid particles ($IrCl_3$/PMMA), apart from characteristic water loss, exhibits two step starting at 270 and 320 °C. The step below 200 °C assigned to head-to-head groups most likely occurred during the spray-drying process in which the applied temperature exceeded 220 °C. The two step process is further confirmed by the evolution of the peaks related to decomposition of PMMA by MS. Similarly, to pure PMMA, we observed the progression of peaks corresponding to MMA (m/z 100) and the products of its own fragmentation (m/z 41, 69). These peaks appear at the same temperatures as in pure PMMA, however, the peak with the maximum at 350°C is much narrower compared to pure PMMA and is slightly shifted toward higher temperatures. The iridium chloride decomposition is observed by appearance of the peaks corresponding to HCl (m/z 36,45), Cl

(m/z 35,45) and CH_3Cl (m/z 50,49). The first (not showed on the graph) has the same shape as the one of Cl but the intensity was twice lower. All these peaks appear at the same temperature and accommodate position between 1st and 2nd step evolution of MMA. Identically to the experiments with pure PMMA, we detected traces of oxygen and nitrogen. Nevertheless, we could discriminate peaks from m/z 28 and m/z 16 occurring at 350°C which corresponds most likely to CO and CH_4.

The MS analysis was further confirmed by FTIR analysis. We observed bands at the same temperature range as in MS measurements. The strongest peaks corresponded well to MMA monomer (like in the case of pure PMMA) and to HCl (series of sharp peaks between 3050-2700 cm^{-1}). Above 3050 cm^{-1} another series of sharp peaks was observed and it could be assigned to CH_4.

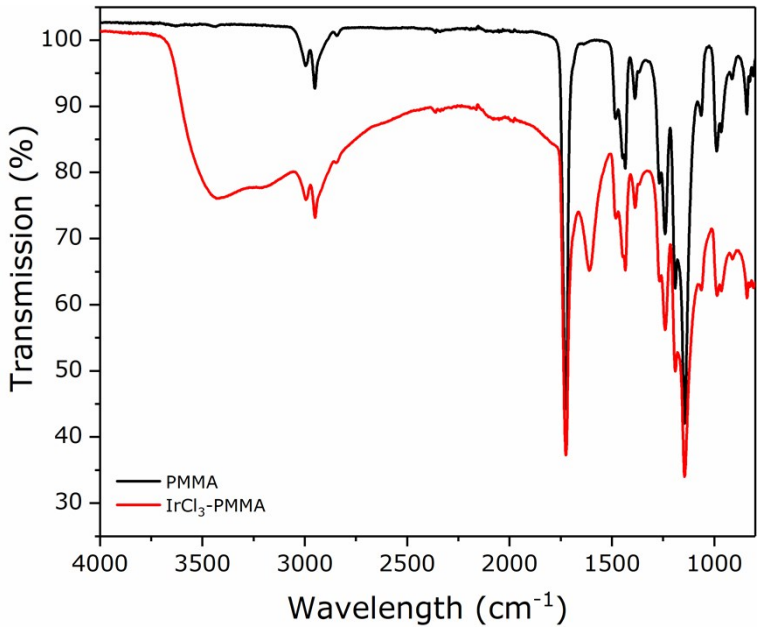

Figure S10 FTIR spectra of PMMA latex beads (black) and hybrid particles after spray drying (red)

The main difference in the FTIR spectra of pure PMMA and spray-dried $IrCl_3$/PMMA is the appearance of two bands in the latter one: i) a very broad band with the maximum at around 3500 cm^{-1} and ii) a sharp peak at 1617 cm^{-1}. Both are very characteristic for adsorbed water molecules, here by $IrCl_3$. The broad band at 3500 cm^{-1} corresponds to the symmetric and asymmetric stretching vibrations and the one at 1617 cm^{-1} originates from bending vibrations of water molecules.

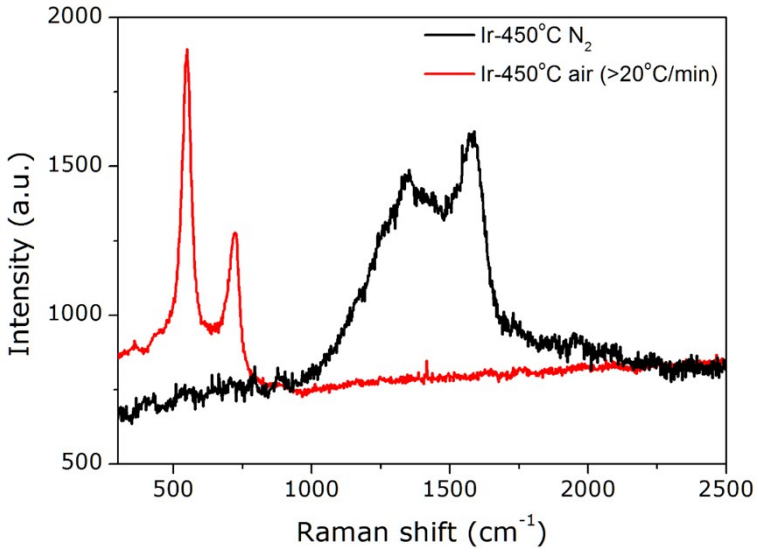

Figure S11 Raman spectra of $IrCl_3$-PMMA calcined at 450°C under either nitrogen (black) or air (red)

Sample calcined in nitrogen shows Raman spectrum with features typical for disordered carbon. So called G peak at 1583 cm^{-1} corresponds to sp^2 carbons, while D peak at 1343 cm^{-1} is linked to breathing modes of carbon rings.[8] Contrary, the spectrum of the sample calcined in air is flat in the same region. However, new bands assigned to Ir-O vibration modes appeared below 1000 cm^{-1}.

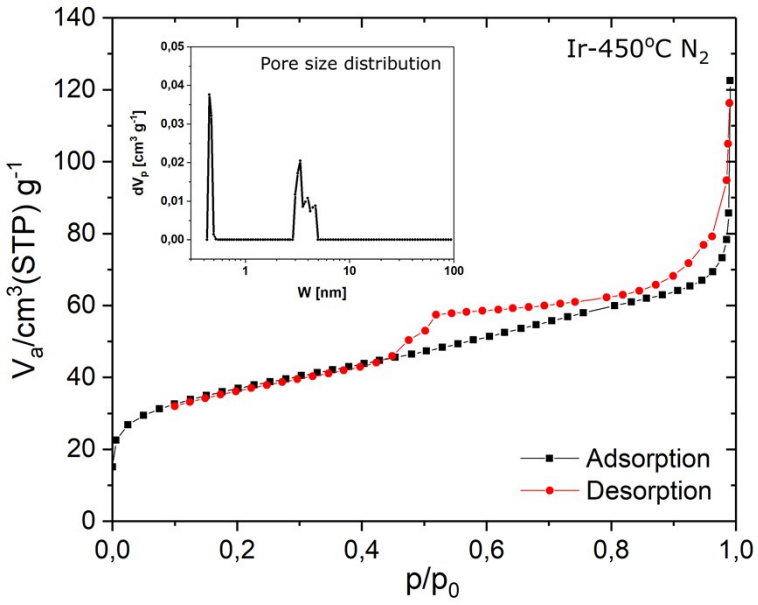

Figure S12 Nitrogen absorption and desorption isotherms of synthesized metallic Ir; pore size distribution calculated by NLDFT method is presented as the inset

.

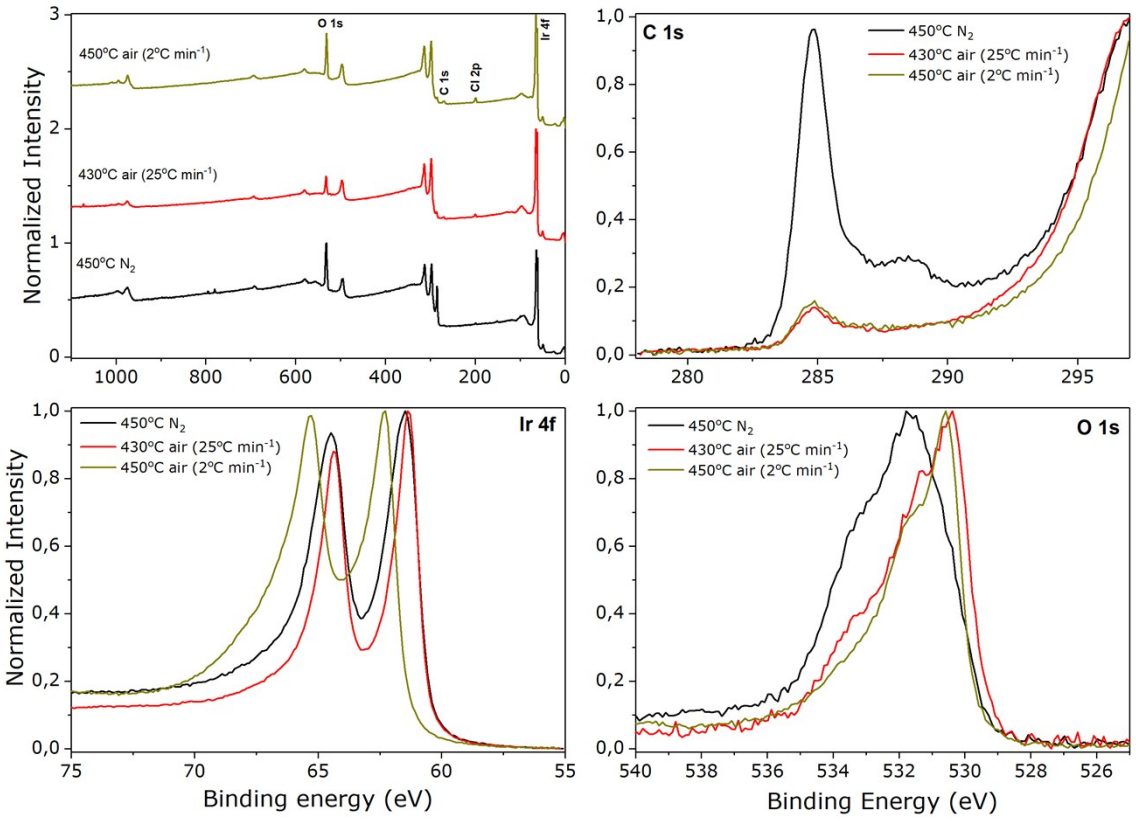

Figure S13 XPS analysis of spray-dried $IrCl_3$/PMMA hybrids calcined in different conditions: survey spectrum and fine analysis of C 1s, Ir 4f and O 1s regions

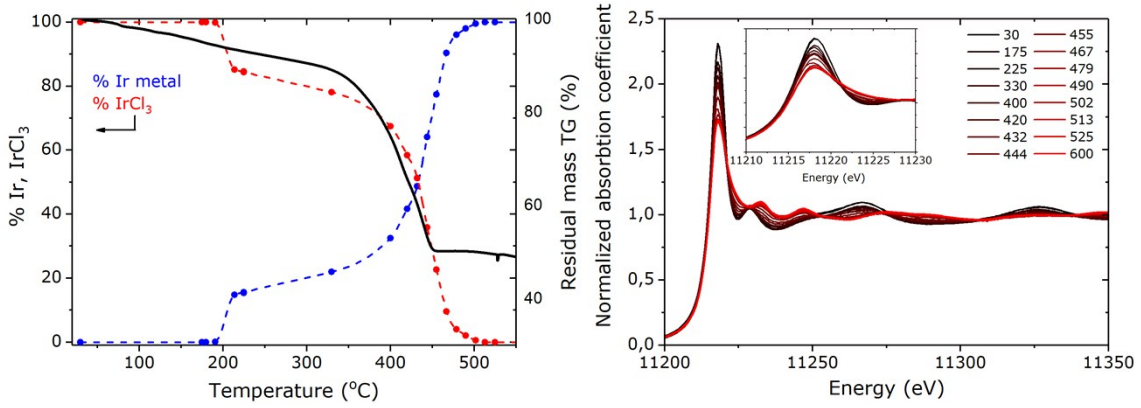

Figure S14 In-situ **structural analysis of $IrCl_3$ spray dried with PS.** a) Combined TGA with the molar percentage of the spray dried $IrCl_3$-like precursor and metallic Ir for mixtures with PS; b) XANES spectra at different temperatures for mixtures with PS

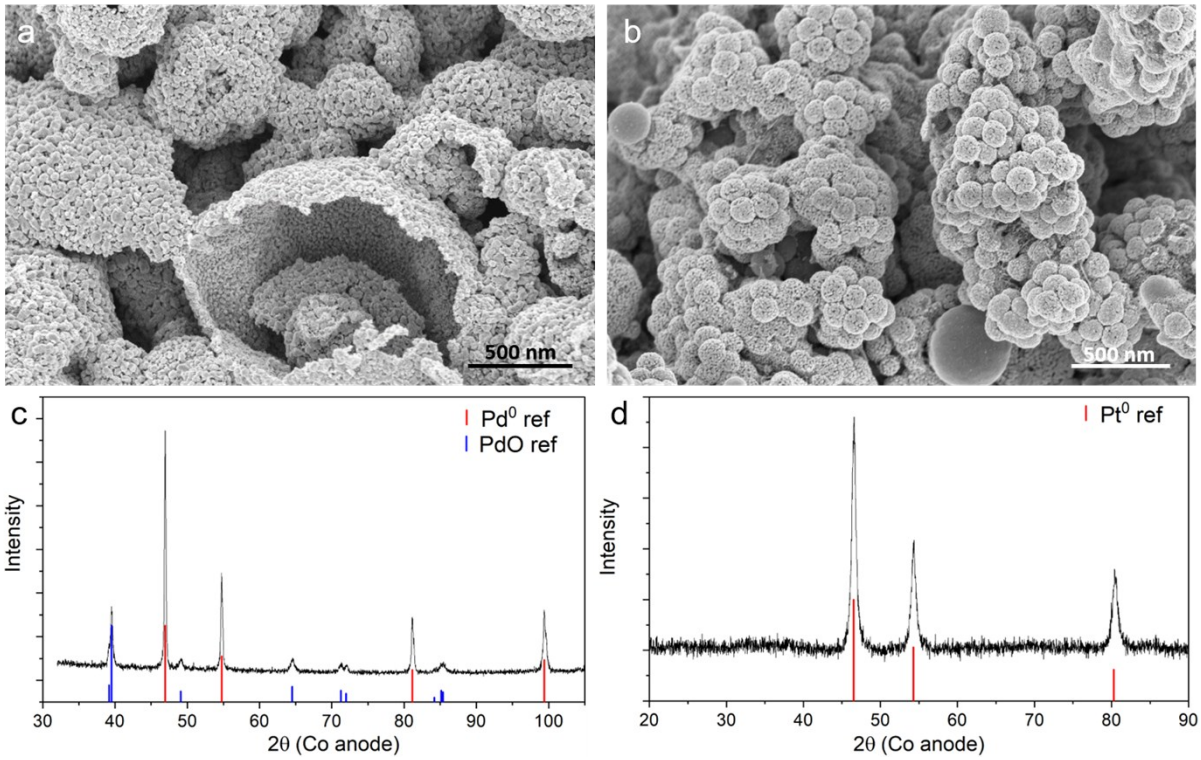

Figure S15 **Spray-dried and calcined in N_2 Pd (450 °C) and Pt (390 °C).** a), c) SEM and XRD of Pd; b), d) SEM and XRD of Pt

After calcination under inert atmosphere, the spray-dried mixtures of Pd salt with PMMA and of Pt salt with PMMA both yield to metallic structures confirming the versatility of the method for the synthesis of porous metals. As for Ru, some oxide impurities are observed for Pd. The morphologies of Pt and Pd particles are however slightly different compared to Ir, Ru and Rh materials. Pd forms porous microspheres in which, unlike for Ir, Ru and Rh, the structuration resulting from PMMA can not be observed; metallic Pt nanoparticles self-arrange into raspberry-like structures. These differences are mainly due to a different interaction between the metal salts and the PMMA during the preparation of the solution before spray-drying. In addition, the growth of particles is strongly enhanced compared to Ir or Rh which modifies the material architecture. Even if the material morphologies slightly differ, the chemical processes leading to the formation of metal under inert atmosphere remain the same for all the noble metals studied.

References

1. Hatton, B., Mishchenko, L., Davis, S., Sandhage, K. H. & Aizenberg, J. Assembly of large-area, highly ordered, crack-free inverse opal films. *Proc. Natl. Acad. Sci.* **107**, 10354–10359 (2010).
2. Blas, H. *et al.* Elaboration of monodisperse spherical hollow particles with ordered mesoporous silica shells via dual latex/surfactant templating: Radial orientation of mesopore channels. *Langmuir* **24**, 13132–13137 (2008).
3. Manring, L. E. Thermal Degradation of Poly(methyl methacrylate). 4. Random Side-Group Scission. *Macromolecules* **24**, 3304–3309 (1991).
4. Manring, L. E. Thermal Degradation of Poly(methyl methacrylate). 2. Vinyl-Terminated

Polymer. *Macromolecules* **22**, 2673–2677 (1989).

5. Manring, L. E., Sogah, D. Y. & Cohen, G. M. Thermal Degradation of Poly(methyl methacrylate). 3. Polymer with Head-to-Head Linkages. *Macromolecules* **22**, 4652–4654 (1989).

6. Briggs, D., Fletcher, I. W. & Goncalves, N. M. Positive secondary ion mass spectrum of poly (methyl methacrylate): a high mass resolution ToF-SIMS study. *Surf. Interface Anal.* **29**, 303–309 (2000).

7. Hsu, H.-J., Kuo, T.-L., Wu, S.-H., Oung, J.-N. & Shiea, J. Characterization of Synthetic Polymers by Electrospray-Assisted Pyrolysis Ionization-Mass. *Anal. Chem.* **77**, 7744–7749 (2005).

8. Ferrari, A. C. *et al.* Raman Spectrum of Graphene and Graphene Layers. *Phys. Rev. Lett.* **97**, 187401 (2006).